Flexoelectro-optic properties of chiral nematic liquid crystals in the uniform standing helix configuration

F. Castles,* S. M. Morris,† and H. J. Coles‡
Centre of Molecular Materials for Photonics and Electronics, Electrical Engineering Division, Department of Engineering, University of Cambridge, 9 JJ Thomson Avenue, Cambridge CB3 0FA, United Kingdom

(Received 6 February 2009; revised manuscript received 30 July 2009; published 18 September 2009)

The flexoelectro-optic effect describes the rotation of the optic axis of a short-pitch chiral nematic liquid crystal under the application of an electric field. We investigate the effect in the uniform standing helix, or "Grandjean" configuration. An in-plane electric field is applied. The director profile is determined numerically using a static one-dimensional continuum model with strong surface anchoring. The Berreman method is used to solve for plane-wave solutions to Maxwell's equations, and predict the optical properties of the resulting structure in general cases. By using a chiral nematic with short pitch between crossed polarizers an optical switch may be generated. With no applied field the configuration is nontransmissive at normal incidence, but becomes transmissive with an applied field. For this case, numerical results using the Berreman method are supplemented with an analytic theory and found to be in good agreement. The transmitted intensity as a function of tilt, the contrast ratio, and the tilt required for full intensity modulation are presented. The angular dependence of the transmission is calculated and the isocontrast curves are plotted. For typical material and cell parameters a switching speed of 0.017 ms and contrast ratio of 1500:1 at normal incidence are predicted, at a switch-on tilt of 41.5 degrees. Experimental verification of the analytic and numerical models is provided.

DOI: 10.1103/PhysRevE.80.031709 PACS number(s): 61.30.Dk, 42.70.Df, 42.79.Kr

I. INTRODUCTION

The bulk optical properties of liquid crystals (LCs) may be manipulated by an applied electric field. Conventionally, this is due to dielectric coupling, where the permanent or induced dipole moments of the molecules tend to align in the applied field. An alternative, more subtle, mechanism was proposed by Meyer in 1969 [1]. The effect, called flexoelectricity, is similar to the piezoelectric effect in ordinary crystals. When an electric field is applied perpendicular to the helical axis of a chiral nematic (N*) LC, flexoelectricity can induce a rotation of the helical axis around an axis parallel to the field. This is known as the flexoelectro-optic effect [2].

While much work has been done on the flexoelectro-optic effect in the uniform lying helix (ULH) configuration, in which the helical axis lies in the plane of the device (see, e.g., Refs. [2–11]), relatively little has been done in the uniform standing helix (USH) configuration, in which the helical axis lies normal to the plane of the device [12–15]. An in-plane electric field provides the flexoelectro-optic tilt, as shown in Fig. 1. The USH configuration is also referred to as the "Grandjean texture."

An N* with pitch P much less than the wavelength λ of light $P \ll \lambda$ behaves like a uniaxial crystal with its optic axis along the helical axis. Hence with no field applied the LC is not birefringent for light at normal incidence and the configuration is nontransmissive between crossed polarizers. When an in-plane electric field is applied at 45° to the polarizers the rotation of the optic axis around an axis parallel to the field causes an induced effective macroscopic birefringence and the configuration will become transmissive. In this way, an optical switch may be generated, as first proposed by Broughton *et al.* [12]. We investigate the optical properties of N* LCs in the USH under the application of an in-plane field, with particular reference to this switching mechanism in the short-pitch limit.

Initially the flexoelectro-optic effect observed was relatively small; in their original paper Patel and Meyer measured a maximum flexoelectro-optic tilt angle of about 7° [2]. Following concerted efforts, highly flexoelectric "bimesogenic" LC materials have been developed [9–11]. Maximum flexoelectro-optic tilt angles of up to 87° have been reported [10], thus enabling the realistic prospect of fabrication of commercial flexoelectro-optic devices such as high-definition LC televisions and monitors.

The response time of the flexoelectro-optic effect τ is governed by the elastic restoring forces of the LC, and can be shown from a hydrodynamic approach to be given by the expression [3]

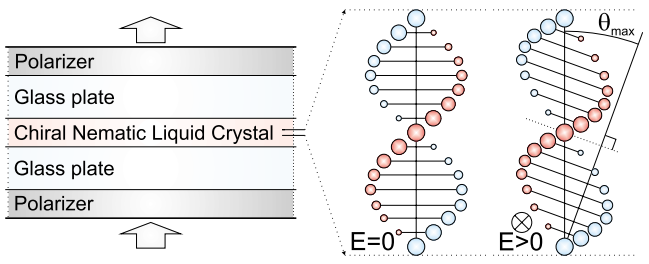

FIG. 1. (Color online) The chiral nematic liquid crystal is confined between glass plates. Planar alignment on the surfaces ensures the uniform standing helix configuration, in which the helical axis is normal to the plates. An in-plane electric field is applied in the same direction as the alignment. Crossed polarizers are aligned at 45° to the direction of the field.

*fc252@cam.ac.uk
†smm56@cam.ac.uk
‡hjc37@cam.ac.uk

$$\tau = \frac{\gamma}{Kk^2}, \tag{1}$$

where k is the helical pitch wave vector $k=2\pi/P$, γ is an effective viscosity, and K is the average of the splay and bend elastic constants of the LC. Switching times are typically of the order of 10^{-5} s for short-pitch N* materials; this is fast enough for incorporation in a device using field sequential color (FSC) generation. FSC has a number of potential advantages due to the fact that a color filter is no longer required, but is hitherto rarely implemented due to the restrictively slow switching of conventional LC devices [16]. Further, the USH configuration is inherently stable and existing planar alignment techniques can be successfully implemented (the ULH is less stable and will usually tend to revert naturally to the USH).

In Sec. II we minimize the free-energy equation, which includes elastic, flexoelectric, and dielectric terms, to determine the director profile of the LC in the USH. The results are compared with the existing results for the ULH. We also investigate the effect that the dielectric anisotropy $\Delta\epsilon$ has on the flexoelectro-optic effect. In Sec. III the optical properties are investigated. The Berreman 4×4 numerical method [17] is used to give general results, which are supplemented with analytic expressions in the short-pitch limit where appropriate. In Sec. III A we investigate the transmission as a function of wavelength for the field-off state and derive an analytic expression for the contrast ratio in the short-pitch limit. In Sec. III B we investigate the electro-optic curves (the transmission as a function of applied field) and their dependence on the material birefringence, the thickness of the LC layer, and the wavelength of light. In addition, the angular dependence of transmission in the field-off and field-on states, and the resultant isocontrast curves are plotted.

II. DIRECTOR PROFILE

Continuum theory [18–20] is used to find the director profile $\mathbf{n}(\mathbf{x})$, a vector field that describes the average molecular orientation at any point $\mathbf{x}$. The director is defined in terms of two polar angles θ and ϕ (conventional notation is shown in Fig. 2).

The general process to find the director profile is as follows: (1) Minimize the free-energy expression using the Euler-Lagrange method to give a set of coupled second-order differential equations—the governing equations. (2) Solve the governing equations, subject to boundary conditions, to give $\mathbf{n}(\mathbf{x})$. We use the expression for the bulk free-energy density, which includes elastic, flexoelectric, and dielectric contributions, $f=f_{\text{elastic}}+f_{\text{flexo}}+f_{\text{dielectric}}$, where

$$f_{\text{elastic}} = \frac{1}{2}K_1(\nabla\cdot\mathbf{n})^2 + \frac{1}{2}K_2(\mathbf{n}\cdot\nabla\times\mathbf{n}+k)^2 + \frac{1}{2}K_3(\mathbf{n}\times\nabla\times\mathbf{n})^2, \tag{2a}$$

$$f_{\text{flexo}} = -\mathbf{E}\cdot[e_1\mathbf{n}(\nabla\cdot\mathbf{n}) - e_3\mathbf{n}\times\nabla\times\mathbf{n}], \tag{2b}$$

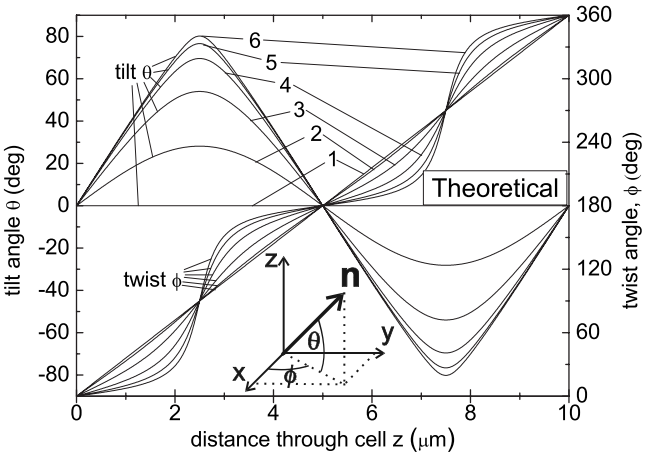

FIG. 2. Average molecular tilt and twist as a function of position for a chiral nematic with one full 2π twist ($t=1$) through a $d=10$ μm thick cell. Values of electric field E (V μm^{-1}) for numbered curves are (1) 0, (2) 0.2, (3) 0.4, (4) 0.6, (5) 0.8, (6) 1. The dielectric anisotropy is set to zero, $\Delta\epsilon=0$.

$$\text{and} \quad f_{\text{dielectric}} = -\frac{\epsilon_0\Delta\epsilon}{2}(\mathbf{E}\cdot\mathbf{n})^2. \tag{2c}$$

Here, K_1, K_2, and K_3 are the splay, twist, and bend Oseen-Frank elastic constants [18,19], $\mathbf{E}$ is the applied electric field, e_1 and e_3 are the splay and bend flexoelectric coefficients, respectively, [21], and $\Delta\epsilon$ is the dielectric anisotropy such that $\Delta\epsilon=\epsilon_\parallel-\epsilon_\perp$, where $\epsilon_\parallel$ and $\epsilon_\perp$ are the parallel and perpendicular components of the dielectric permittivity, relative to the director, respectively [22].

Assuming the thickness of the LC layer to be small, and the electric field to be uniform (i.e., ignoring fringing effects), there will be no variation in the director in, say, the x and y directions. In this case the model becomes one dimensional and the director is then a function only of z with $\theta=\theta(z)$, $\phi=\phi(z)$, and $\mathbf{n}=\mathbf{n}(z)$. We note that our method is similar to that in Ref. [14], which uses the Ericksen-Leslie theory with flow. It is assumed that $\mathbf{E}=(E,0,0)$ is constant due to the applied (static) electric field and not affected by depolarization fields. Strong anchoring is used, with boundary conditions

$$\theta(0)=\theta(d)=\phi(0)=0, \quad \phi(d)=2\pi t, \tag{3}$$

where the twist number t gives the number of full 2π rotations of the director across the cell thickness d. In each case we assume $Pt=d$ and that for highly flexoelectric materials there is no unwinding of the helical structure.

The governing equations were solved numerically, to give what may be called the "exact" numerical solutions for the director profile in terms of the angles $\theta(z)$ and $\phi(z)$, (with maximum absolute error set to 10^{-6} rad in this paper). The input material parameters shown in Table I are used throughout this paper, and may be considered representative of some highly flexoelectric, pure, bimesogenic LCs (see e.g., Refs. [11,23]).

The director profile is shown in Fig. 2. For clarity we consider here only one twist of N* across the cell. The direc-

TABLE I. Throughout this work we use the following material parameters for theoretical predictions. They are based on experimental measurements of pure bimesogenic liquid crystals from Refs. [11,23].

Material parameter	Symbol and value
splay elastic constant	$K_1=6$ pN
twist elastic constant	$K_2=2$ pN
bend elastic constant	$K_3=7$ pN
average flexoelectric coefficient	$\bar{e}=\frac{(e_1-e_3)}{2}=10$ pC m^{-1}
viscoelastic ratio	$\frac{\gamma}{K}=1.5\times10^{10}$ m^{-2} s

tor profile for a multipitch device is a repetition of this shape. To isolate the effect of flexoelectricity, from the dielectric reorientation, $\Delta\epsilon$ is initially set to zero. (This has been shown to be a valid approximation for some bimesogenic LCs [24]).

The result of the flexoelectric distortion in short-pitch N*s is to effectively rotate the optic axis in a positive sense about the direction of the applied field. The angle of this rotation is given by the maximum value of the tilt $\theta_{\max}$, the figure of merit for the flexoelectro-optic effect (note that this angle is also commonly denoted as ϕ; however we have already used ϕ to denote the azimuthal angle of the director).

It is instructive to see how our results, from the full numerical solution to the governing equations, compare with the existing expressions for the flexoelectro-optic distortion, which were derived for the ULH geometry. Assuming that the director rotates uniformly about the new helical axis in the ULH, the following equation may be derived for the maximum tilt angle $\theta_{\max}$ (see, e.g., Refs. [2,4,25]):

$$\tan\theta_{\max}=\frac{e_1-e_3}{2K_2k}E-\frac{K_1-2K_2+K_3}{2K_2}\sin\theta_{\max}, \tag{4}$$

which we may call the "ULH expression." In the limit of small values of $\theta_{\max}$ this leads to the ubiquitous expression for the tilt [2],

$$\tan\theta_{\max}\approx\frac{(e_1-e_3)E}{(K_1+K_3)k}. \tag{5}$$

We may call this second expression the "tan approximation" to $\theta_{\max}$. Figure 3 shows that our results from the full solution to the governing equations in the USH accurately match those from the ULH expression for this particular geometry (i.e., for the case in which the LC is aligned in the direction of the electric field at the boundaries). It is also seen that both results increasingly deviate from the tan approximation expression as the electric field is increased. For this case, we find the exact rotation of the optic axis is of the order of 10° larger than that predicted by the tan approximation at tilts $\gtrsim$60°.

While we find that the ULH expression given in Eq. (4) is accurate in this particular case, the method used in this paper, based on the full numerical solutions to the governing equations, is a much more powerful and general method in the USH configuration. In particular, it can deal with the situation in which the electric field is not along the molecular direction at the boundaries and the case for which $\Delta\epsilon\neq0$. The effect on the flexoelectro-optic effect of re-introducing the dielectric anisotropy has also been investigated and plotted in Fig. 3. It is found that the dielectric anisotropy increasingly suppresses the flexoelectro-optic tilt. This may be explained by the fact that under the application of an in-plane field, the dielectric anisotropy tends to align the molecules in the direction of the field, while the flexoelectro-optic coupling tends to rotate the molecules, in general, away from the planar confinement.

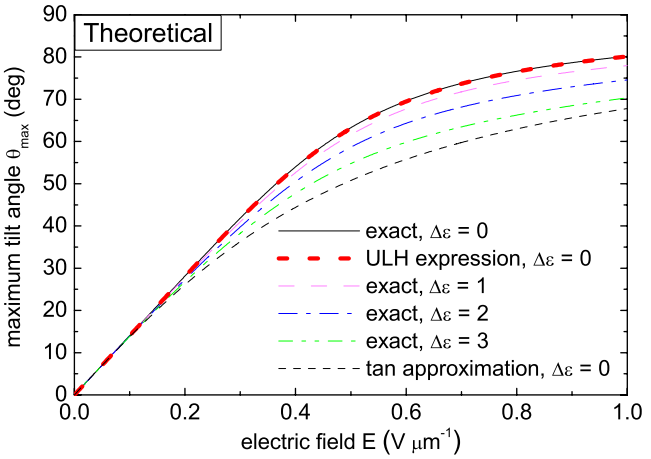

FIG. 3. (Color online) Maximum tilt angle $\theta_{\max}$ as a function of electric field E for a chiral nematic with one full 2π twist ($t=1$) through a $d=10$ μm thick cell. The exact solutions to the free-energy equations, for various values of dielectric anisotropy $\Delta\epsilon$, are compared against solutions from the ULH expression, Eq. (4), and the tan approximation, Eq. (5).

III. OPTICAL PROPERTIES

The optical properties may be accurately investigated using the Berreman 4×4 method [17]. This includes the effect of selective Bragg reflection and may be used for light at oblique angles of incidence. Excellent agreement has previously been found between the Berreman method and experimental results, and it is regarded as an accurate predictive tool (see, e.g., Ref. [26]). The method leads to numerical solutions, valid for general values of P and λ in our model. Increased precision is achieved by increasing the number of slices into which the sample is decomposed for computation [27]. Polarizers were implemented into the analysis using the "equivalent polarizer" method [28]. In this paper we seek to investigate only the optical properties of the LC layer itself. To reduce reflection at the first LC boundary the refractive index of the isotropic medium in which the LC is situated is set equal to the refractive index of the LC at the boundary in the direction of the first polarizer. It is noted that an extension of the method to include the effect of the glass and alignment layers would be expected to increase the accuracy of the predictions [26], but is not considered here. In the limit that $P\ll\lambda$ we may derive analytic expressions for the optical properties.

A. Field-off state

First, we investigate the intensity transmission of light at normal incidence in the field-off state, in which case the LC

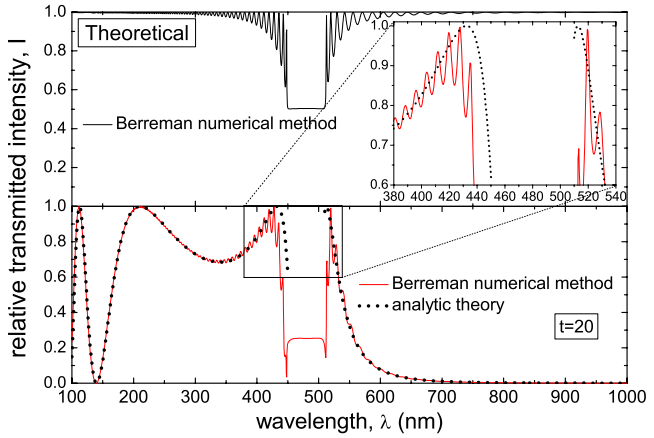

FIG. 4. (Color online) The transmitted intensity as a function of wavelength in the field-off state for a $t=20$ twist cell (lower graph), and the photonic band gap of the same chiral nematic material without an analyzer (upper graph). Outside the selectively reflective region the analytic expression, derived using the de Vries equation, Eq. (7), is shown to approximate the exact numerical results calculated using the Berreman method. ($d=6$ μm, $n_{\parallel}=1.7$, and $n_{\perp}=1.5$.)

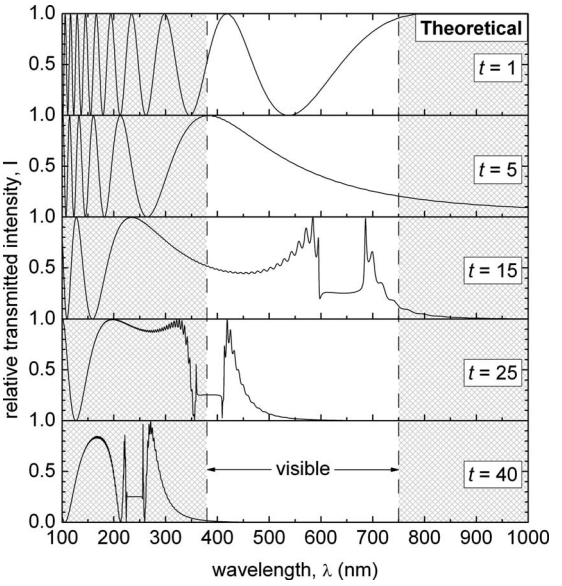

FIG. 5. The transmitted intensity as a function of wavelength in the field-off state for various numbers of twist of the chiral nematic t, calculated using the Berreman method. As t is increased above about $t=30$ (and pitch P is thus reduced) the selectively reflective region is pushed below visible wavelengths, and the transmission in the visible region decreases. $d=6$ μm, $n_{\parallel}=1.7$, and $n_{\perp}=1.5$.

structure is that of an undistorted N^*. Using the Berreman method, the typical transmission as a function of wavelength λ is shown in Fig. 4, normalized to the intensity of light passing through the first polarizer. The transmission spectrum with no analyzer (second polarizer) present is also plotted to show clearly the selectively reflective region. For a multitwist sample such as this there are three main regions: (1) an oscillating region at shorter wavelengths, (2) a complicated transmission pattern in and around the range of selectively reflected wavelengths of the N^*, and (3) a sharp fall in transmission at larger wavelengths. The range of selective reflection is given by $Pn_{\perp}<\lambda<Pn_{\parallel}$, where $n_{\parallel}$ and $n_{\perp}$ are the local refractive indices relative to the local director. Outside the selectively reflective region we may use the de Vries equation [29] to derive an approximate analytic expression for the transmission. The de Vries equation provides an expression for the angle of rotation Ψ per unit distance z of plane-polarized incident light (though the transmitted light is elliptically polarized),

$$\frac{\partial\Psi}{\partial z}=-\frac{2\pi}{P}\frac{\beta^2}{8\lambda'(1-\lambda'^2)}, \tag{6}$$

where $\beta\equiv(n_{\parallel}^2-n_{\perp}^2)/(2\bar{\epsilon})$, $\lambda'\equiv\lambda/(P\sqrt{\bar{\epsilon}})$, and $\bar{\epsilon}\equiv(n_{\parallel}^2+n_{\perp}^2)/2$. Between crossed polarizers the transmitted intensity I_{off} is given in terms of the angle of rotation Ψ by $I_{\text{off}}=\sin^2\Psi$, giving

$$I_{\text{off}}=\sin^2\left(-\frac{\pi(\Delta n)^2Pd}{4\lambda^2\left(1-\left(\frac{\lambda}{\bar{n}P}\right)^2\right)}\right), \tag{7}$$

for $\lambda\lesssim n_{\perp}P$ or $\lambda\gtrsim n_{\parallel}P$, where $\bar{n}\equiv(n_{\parallel}+n_{\perp})/2$, $\Delta n\equiv n_{\parallel}-n_{\perp}$, and we have used the approximation (used in the derivation of the de Vries equation) that β is small and hence $\bar{n}\approx\sqrt{\bar{\epsilon}}$. The accuracy of this analytic expression increases as we move away from the selectively reflective region, as shown by the dotted line in Fig. 4.

Figure 5(a) shows the effect of increasing the number of twists t of N^* across the device while keeping the cell thickness and the local material birefringence constant, using the Berreman method. It is seen that as the number of twists increases (and the pitch is thus reduced) the selectively reflective region is pushed into the ultraviolet and the transmission in the visible region is reduced. As expected, if we wish to use the device as an optical switch that is off when no voltage is applied, we must use a high-twist short-pitch N^* such that $Pn_{\parallel}\lesssim\lambda_{\text{min}}$, where λ_{min} is the lower edge of the range of operational wavelengths.

Figure 6 provides experimental verification of the predicted behavior. The transmitted intensity as a function of λ was measured using a spectrometer. Photographs of test cells confirm that, as the pitch is reduced, a uniform dark state is observed between crossed polarizers ($d=5$ μm). The nematic liquid crystal material BL003 (Merck KGaA) was used, with varying concentrations of chiral dopant BDH1281 (Merck KGaA), to produce equivalent samples with differing P. One such sample was analyzed in a "wedge cell" with nonuniform d, as shown in Fig. 6(b). It is qualitatively confirmed that as d is reduced, I_{off} is reduced, as predicted by Eq. (7).

In the limit $P\bar{n}\ll\lambda$, Eq. (7) may be further simplified to give the transmitted intensity as

$$I_{\text{off}}\approx\frac{\pi^2\bar{n}^4(\Delta n)^4P^6d^2}{16\lambda^8}, \quad \text{for} \quad P\bar{n}\ll\lambda. \tag{8}$$

As a simple indication of the efficiency of the switching mechanism, we may define the contrast ratio C of the device

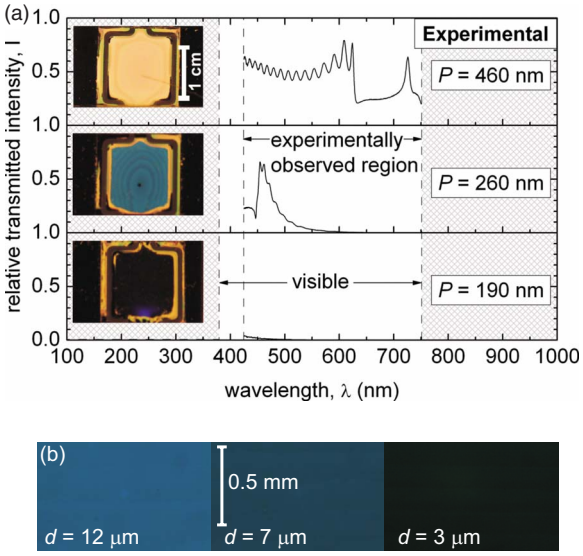

FIG. 6. (Color online) (a) Experimental spectra verify the important features of Fig. 5. Photographs confirm that, as the pitch is reduced, a uniform dark state is observed between crossed polarizers ($d=5$ μm). (b) Optical micrographs confirm that the transmitted intensity between crossed polarizers is reduced as the thickness of the liquid crystal layer is reduced ($P=190$ μm), as predicted by Eq. (7).

to be the ratio of the transmitted intensity in the "on" state I_{on} to that in the "off" state I_{off}. We show in the following section that the field-on state will be such that $I_{on}=1$ for light at normal incidence (the intensity at the peak of the electro-optic curve), giving

$$C \equiv \frac{I_{on}}{I_{off}} = \frac{1}{I_{off}}, \tag{9}$$

where I_{off} is given by Eq. (7) or Eq. (8) in the appropriate limit.

B. Field-on state: Electro-optics

1. Berreman method numerical results

For the case described above for which $P\bar{n} \ll \lambda$, and the device is nontransmissive when no field is applied, we now investigate the transmitted intensity as a function of the applied electric field. We vary, in turn, the local material birefringence Δn, the device thickness d, and the wavelength of incident light λ. Default device parameters are as given in Table II.

The transmission as a function of electric field using the Berreman method is shown in Fig. 7 for three values of local material birefringence $\Delta n=0.1, 0.2, 0.3$ (obtained by varying $n_{\parallel}$ and keeping $n_{\perp}=1.5$ constant). It is seen that as Δn increases, the flexoelectro-optic tilt angle required for full intensity modulation to occur is decreased.

The effect of increasing the device thickness $d=4, 6, 8$ μm while holding constant λ, Δn, and t is shown in Fig. 8. Increasing the device thickness is found to decrease the flexoelectric tilt angle required for full intensity modulation.

TABLE II. The dependence of the optical properties on the parameters Δn, d, λ, and t is investigated theoretically. In each case the other variables are held constant at the following default values.

Parameter	Symbol and value
$\perp$ component of local refractive index	$n_{\perp}=1.5$
$\parallel$ component of local refractive index	$n_{\parallel}=1.7$
Cell thickness	$d=6$ μm
Wavelength of light	$\lambda=532$ nm
Number of N* twists	$t=40$ $(t=d/P)$

Finally, we investigate the wavelength dependence of the transmission at constant Δn, t, and d, as shown in Fig. 9 for blue ($\lambda=448$ nm), green ($\lambda=532$ nm), and red ($\lambda=632.8$ nm) light. It is found that the flexoelectric tilt angle required for full intensity modulation is lower for shorter wavelengths.

We find that, in the limit $P\bar{n} \ll \lambda$, varying t has no effect on the transmission as a function of tilt. However, the tilt for a given electric field strength will vary.

2. Analytic formulation

In the limit $\bar{n}P \ll \lambda$ it is possible to derive an analytic expression for the transmission as a function of tilt. In this limit, where the molecular director rotates rapidly compared to the wavelength of light, light will not discern the helical molecular configuration but instead be affected by the average refractive index of the rotating director. Hence the N* may be considered a uniaxial birefringent material with optic axis along the helical axis. $n_{\parallel}$ and $n_{\perp}$ are the local material refractive indices, i.e., they are the refractive indices of the equivalent nematic (N) from which the N* is composed. If the molecules are locally oriented in the x direction, then the local material optical indicatrix is defined by the ellipsoid

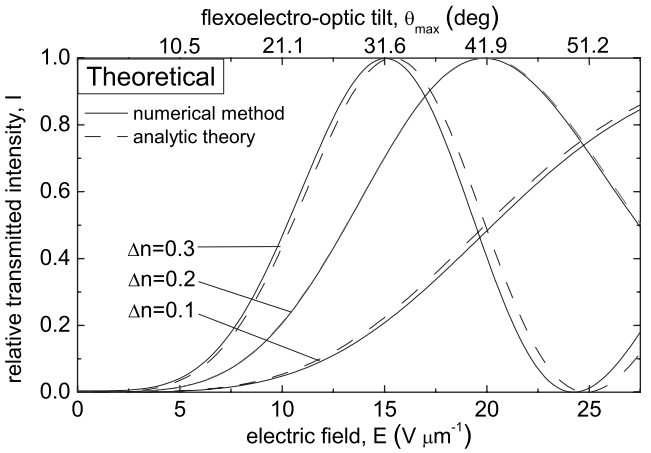

FIG. 7. Electro-optic curve, showing transmission as a function of applied field (bottom axis) and as a function of flexoelectro-optic tilt (top axis), for three values of Δn (obtained by varying $n_{\parallel}$ and keeping $n_{\perp}=1.5$ constant). Increasing the local material birefringence is seen to decrease the switch-on electric field.

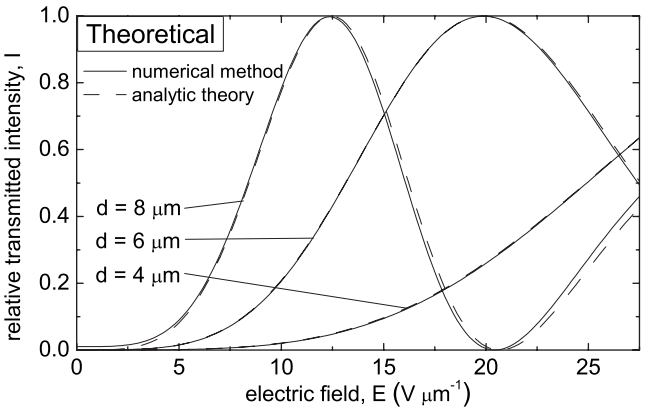

FIG. 8. Electro-optic curve, showing transmission as a function of applied field for three values of device thickness d. Increasing the device thickness is seen to decrease the switch-on electric field.

$$\frac{x^2}{n_\parallel} + \frac{y^2}{n_\perp} + \frac{z^2}{n_\perp} = 1. \tag{10}$$

The refractive index for light traveling along the z axis, and polarized at an angle θ' to the x axis, is given from the optical indicatrix as

$$n(\theta') = \left[\left(\frac{\cos\ \theta'}{n_\parallel} \right)^2 + \left(\frac{\sin\ \theta'}{n_\perp} \right)^2 \right]^{-1/2}. \tag{11}$$

As the director rotates about the z axis the z component of the refractive index will be unaffected (and equal to $n_\perp$), but the refractive index in the x-y plane will be some kind of average of $n_\parallel$ and $n_\perp$. If we denote this average as n_{eff}, the effective optical indicatrix for the short-pitch N* is defined by

$$\frac{x^2}{n_{\text{eff}}} + \frac{y^2}{n_{\text{eff}}} + \frac{z^2}{n_\perp} = 1. \tag{12}$$

The local material indicatrix is a prolate ellipsoid while the effective N* indicatrix is an oblate ellipsoid. The average, n_{eff}, is determined by integrating $n(\theta')$ over one rotation,

$$n_{\text{eff}} = \frac{1}{2\pi} \int_0^{2\pi} n(\theta') d\theta', \tag{13}$$

$$= \frac{1}{2\pi} \int_0^{2\pi} \left[\left(\frac{\cos\ \theta'}{n_\parallel} \right)^2 + \left(\frac{\sin\ \theta'}{n_\perp} \right)^2 \right]^{-1/2} d\theta'. \tag{14}$$

This gives

$$n_{\text{eff}} = \frac{2}{\pi} n_\parallel \bar{K} \left(\sqrt{\frac{n_\perp^2 - n_\parallel^2}{n_\perp^2}} \right), \tag{15}$$

where $\bar{K}$ is the complete elliptic integral of the first kind (see, e.g., Ref. [30] for a discussion of $\bar{K}$). A number of expressions for n_{eff} approximate to Eq. (15) exists in the literature, such as $n_{\text{eff}}^2 = (n_\parallel^2 + n_\perp^2)/2$ (see, e.g., Ref. [31]).

Under the flexoelectro-optic distortion the shape of the effective optical indicatrix is unchanged, but it is rotated by $\theta_{\max}$ about the axis of direction of the field. Using Jones matrices, the transmitted intensity between crossed polarizers can be shown to be

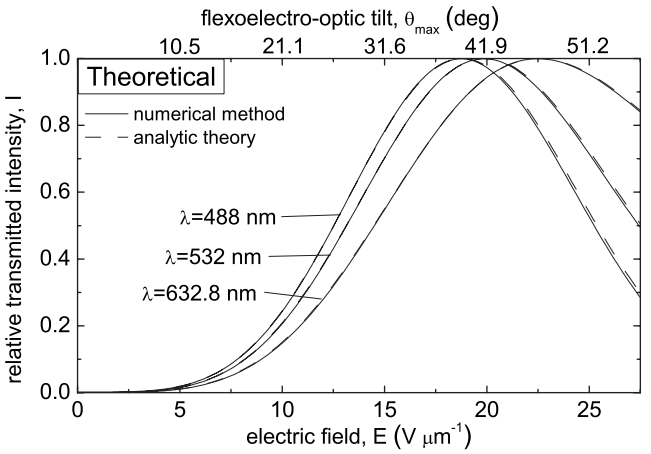

FIG. 9. Electro-optic curve, showing transmission as a function of applied field (bottom axis) and as a function of flexoelectro-optic tilt (top axis), for red, green, and blue wavelengths of light. The switch-on voltage is seen to be lower for shorter wavelengths.

$$I = \sin^2 \frac{\delta}{2}, \tag{16}$$

where $\delta = 2\pi d \Delta n / \lambda$, and Δn is now a function of the tilt $\theta_{\max}$, as determined from the effective indicatrix for the N* in Eq. (12). For normally incident light

$$\Delta n(\theta_{\max}) = \left[\left(\frac{\cos\ \theta_{\max}}{n_{\text{eff}}} \right)^2 + \left(\frac{\sin\ \theta_{\max}}{n_\perp} \right)^2 \right]^{-1/2} - n_{\text{eff}}. \tag{17}$$

The electro-optic curves predicted by this analytic expression, with n_{eff} as determined by Eq. (15), are plotted in Figs. 7–9 as dotted lines. The small discrepancy between the analytic and the numeric curves may be due to the fact that the analytic method is only exactly correct in the short-pitch limit $\bar{n} P / \lambda \to 0$.

The tilt required for full intensity modulation is found by solving $\delta/2 = -(2n+1)\pi/2$ for $n = 0, 1, 2, \ldots$, giving

$$\theta_{\max}^{FI} = \sin^{-1} \left\{ \left[\frac{1/(\lambda(2n+1)/2d - n_{\text{eff}})^2 - 1/n_{\text{eff}}^2}{1/n_\perp^2 - 1/n_{\text{eff}}^2} \right]^{1/2} \right\}. \tag{18}$$

3. Experiment

The experimental electro-optic curve is shown in Fig. 10. The in-plane field was generated using an interdigitated (indium tin oxide) electrode pattern on one of the glass surfaces. $d = 5\ \mu$m, the width of the electrodes was 5 μm, and the distance between electrodes was 15 μm. A mixture of bimesogenic materials was used [10] ($P \approx 150$ nm), and the experiment was carried out at a temperature of 30 °C. A bipolar square-wave signal of frequency 1 kHz was applied. It is seen that an optical switch is generated as predicted. Throughout the plotted region the texture reverted to the original off state upon removal of the electric field on a time scale of ~0.1 ms. In this range the shape of the curve is in

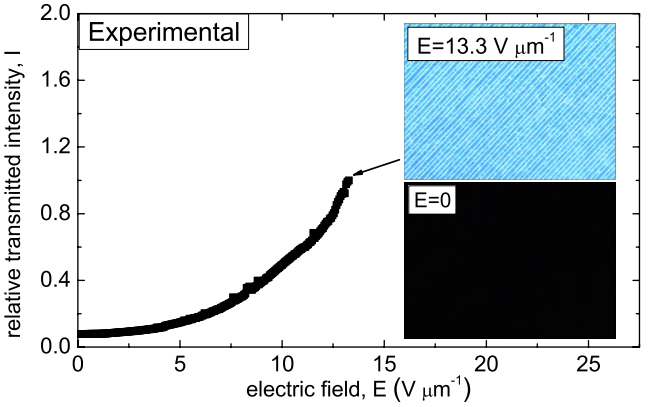

FIG. 10. (Color online) Experimental electro-optic curve, showing transmission as a function of applied electric field. In the measured range, the shape of the curve matches the theoretical prediction.

general qualitative agreement with Figs. 7–9. The curve is truncated because, for the material used, at too high fields the texture became distorted and did not represent a valid flexoelectro-optic switch.

4. Angular dependence and isocontrast curves

The dependence of the transmission on the angle of incidence of light in air is plotted in Fig. 11 for the field-off and field-on states. In order to focus on the optical properties of the LC layer itself, we ignore additional reflections at the glass boundaries. The refractive index of the glass is set equal to the refractive index of the LC in the direction of the first polarizer at the boundary ($n_{\text{glass}} \approx 1.59$). The polar angle in glass α_{glass} is converted to that in air α_{air} according to Snell's law, $\alpha_{\text{air}} = \sin^{-1}(n_{\text{glass}} \sin \alpha_{\text{glass}})$. For the field-on state the electric field value of $E = 19.8$ V μm^{-1} is used, as determined from Fig. 7, to give full intensity at normal incidence. The angular dependence of the contrast ratio is plotted in Fig. 12. The material and cell parameters are as given in Tables I and II. This configuration gives a contrast ratio at normal incidence of $C = 1500$.

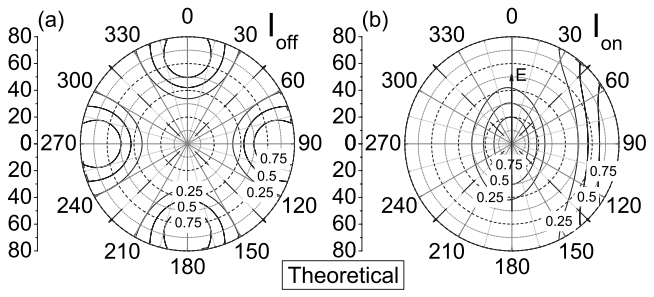

FIG. 11. Contour plots showing angular dependence of relative transmission in the (a) field-off and (b) field-on states ($E = 19.8$ V μm^{-1}). Lines denote equal intensity contours. Material and cell parameters are as given in Tables I and II. The in-plane electric field is applied at zero azimuthal angle, while the crossed polarizers are at $\pm 45°$.

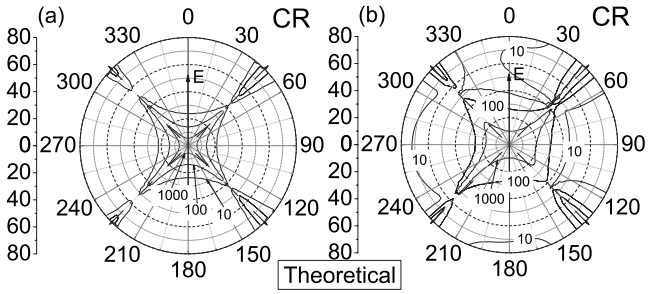

FIG. 12. Isocontrast curves: contrast ratio C as a function of angle of incidence of light: (a) uncompensated and (b) c-plate compensated. Lines denote equal C contours. At normal incidence $C = 1500$.

C. Practical considerations

1. Issues of uniformity

Throughout this work, for simplicity and clarity, our theory has assumed a homogeneous in-plane electric field. In device applications the field will be, to some degree, nonhomogeneous. The in-plane field is typically generated by a thin (~100 nm) layer of metal (e.g., chromium), forming an interdigitated electrode pattern. This produces an electric field of approximate uniformity in a region between the electrodes, with fringing fields relevant near the electrodes themselves. The uniformity of the field between the electrodes will be primarily dependent on the ratio of the electrode spacing d_e to the device thickness d. Current devices that use in-plane switching mechanisms indicate that a ratio in the range $d_e/d \approx 2-5$ is acceptable for display applications. Our assumption of uniformity appears to be somewhat validated by the qualitative agreement of the theory and experiment. The effect of fringing fields may be explicitly taken into account using a two- or three-dimensional model; however this is beyond the scope of the present work. We note that the network of defects that may be generated above the electrodes need not affect the optical properties of the device because the electrodes may be opaque.

We have also assumed a monodomain USH sample. Over a large area, small fluctuations in the device thickness will lead to domains with small variations in the number of twists t (integer and half-integer values of t are allowed). This will not have an unduly large effect on the operation of the device for three reasons: (1) Even with small variations in t, the device will still appear black in the off state. (2) The tilt angle required for full intensity modulation is independent of t, as shown using the Berreman method, and expected using the analytic theory—once the N^* is in the regime $P \ll \lambda$, the effective refractive index is fixed, regardless of t or P. (3) While the electric field required for a given tilt angle will depend on P, there will not be a significant deviation in P between the domains. Indeed, the separate domains, with differing t, exist so as to minimize the variation in P when small deviations in d are present. The maximum fractional variation in the pitch is given by $\Delta P = 1/(4t)$. Taking the typical value $t = 40$ gives $\Delta P = 0.006\,25$. By observing the peak of the electro-optic curve, this results in a typical variation in the transmitted intensity in the on state, due to twist-

jump domains, of $\lesssim 0.1\%$. A more direct consequence of fluctuations in d is due to the variation in the thickness of optically active material itself: an effect common to all LC devices. The error tolerance on d in standard commercial display devices is $\sim \pm 250$ nm. Investigating the effect of such variations in the current device using Eq. (16) reveals that the variation in the transmitted intensity in the on state is $\sim 0.4\%$.

In addition, the flexoelectro-optic tilt angle has been shown to be essentially independent of temperature (see, e.g., Ref. [6]).

2. Device optimization

Our results show that to optimize the flexoelectro-optic effect for use as an optical switch, a number of competing factors must be considered. As the pitch is reduced, the contrast ratio of the device increases, so for a high contrast ratio we desire a short pitch. Similarly, for a fast response time a short pitch is desired, according to Eq. (1), which shows $\tau \propto P^2$. However, the electric field required for a given flexoelectro-optic tilt also depends on the pitch according to Eq. (4). Thus, a large pitch is desired for a low switch-on field. Hence a practical compromise must be found. In this paper we have presented results on a configuration that produces a high contrast ratio, resulting in electric fields that are, by necessity, higher than those sometimes quoted [10].

Similarly, while a small birefringence and small cell thickness are desired for a good contrast ratio, a large birefringence and large cell thickness will provide full intensity modulation at smaller tilt angles and lower electric field values. Further, while a configuration that needs only a small tilt angle for full intensity modulation will lead to a lower switch-on field, a large tilt angle will lead to a wide viewing angle. Again, a practical compromise must be found.

The driving voltage V_{on} may be approximately obtained according to $V_{\mathrm{on}}=E_{\mathrm{on}}\times d_{\mathrm{e}}$, where E_{on} is the electric field required for full intensity modulation, and d_{e} is the in-plane electrode separation (see, e.g., Ref. [15] for a discussion of the accuracy of this expression). Hence a small electrode separation is required for a low driving voltage yet, as previously discussed, a large electrode separation is desirable to provide a more uniform electric field.

While the characteristics are strongly dependent on the device parameters, it is instructive to look at a particular example. Using the material and cell parameters as shown in Tables I and II, we predict a response time as defined by Eq. (1) of $\tau=8.5$ μs. This is the time taken for the tilt to fall to $1/e$ of its original value. To convert to the time for the tilt to fall from 90% to 10% we may approximately double τ to give $\tau_{90-10}\approx 17$ μs. The Berreman method computes the contrast ratio at normal incidence to be $C=1500$, at a switch-on tilt of 41.5° attained at an electric field value of $E_{\mathrm{on}}=19.8$ V $\mu\mathrm{m}^{-1}$. Other device parameter configurations may give a much lower switch-on field, but with an associated loss of contrast. The material parameters were chosen based on experimental data for pure bimesogenic materials. We note that mixtures of bimesogenic LCs can lead to increased flexoelectric coefficients [10], which would result in lower fields required for the optical switch.

It is seen in Figs. 11 and 12 that the transmission through the device has a strong angular dependence. The angular dependence may be improved to acceptable levels using a birefringent optical compensation film (an analogy may be drawn here with the vertically aligned nematic display device [32]). As a simple example of this, a uniaxially birefringent compensation film, with optic axis perpendicular to the plane of the device, is implemented and found to widen the viewing angle—Fig. 12(b). The film is chosen such that its phase retardation approximately cancels that of the LC layer, thus reducing light leakage at non-normal angles of incidence in the field-off state. For simplicity, the thickness of the compensation film was set equal to the thickness of the LC layer and the birefringence was set to $\Delta n_{\mathrm{film}}=-\Delta n_{N*}$, where $\Delta n_{N*}=n_{\perp}-n_{\mathrm{eff}}$ is the effective birefringence of the N^* in the short-pitch limit.

IV. CONCLUSION

We have investigated the properties of the flexoelectro-optic effect in the USH geometry using a combination of numerical modeling, analytic theory, and experiment. The model, based on numerical solutions to the governing equations, is capable of including the effects of nonzero dielectric anisotropy and arbitrary (strong) boundary orientations. We find that the dielectric anisotropy suppresses the flexoelectro-optic tilt. For the special case in which the electric field is aligned along the director at the boundary, the effect is almost identical to that in the ULH. For zero dielectric anisotropy the flexoelectro-optic tilt angle may be given by Eq. (4). For large tilts ($\gtrsim 60°$) we find considerable deviation from the ubiquitous expression for the tilt, Eq. (5), (of the order of 10°). Thus for large tilts we advocate the use of one of the more accurate methods.

For small N^* pitch, it is possible to form an electro-optic switch between crossed polarizers. We investigated the optical properties of the flexoelectro-optic effect in the USH with particular reference to this switching mechanism. As $\bar{n}P/\lambda \rightarrow 0$ the N^* becomes optically isotropic for light traveling along the helical axis, creating a "dark" state between crossed polarizers when no electric field is applied. The efficiency of the optical switch is primarily dependent on how dark this state is, and may be quantitatively described by the contrast ratio, which is determined as a function of the material and cell parameters according to Eqs. (7)–(9).

We investigated the transmitted intensity as a function of applied electric field for various Δn, d, and λ. An analytic expression for the transmitted intensity as a function of tilt was derived [Eqs. (16) and (17)], and found to support the Berreman 4×4 method results.

ACKNOWLEDGMENTS

We would like to thank the Engineering and Physical Sciences Research Council (U.K.) for financial support. We acknowledge the help of Damian Gardiner and Qasim Malik. One of the authors (F.C.) gratefully acknowledges Merck.

[1] R. B. Meyer, Phys. Rev. Lett. **22**, 918 (1969).
[2] J. S. Patel and R. B. Meyer, Phys. Rev. Lett. **58**, 1538 (1987).
[3] J. S. Patel and S.-D. Lee, J. Appl. Phys. **66**, 1879 (1989).
[4] S.-D. Lee, J. S. Patel, and R. B. Meyer, J. Appl. Phys. **67**, 1293 (1990).
[5] L. Komitov, S. T. Lagerwall, B. Stebler, and A. Strigazzi, J. Appl. Phys. **76**, 3762 (1994).
[6] P. Rudquist, M. Buivydas, L. Komitov, and S. T. Lagerwall, J. Appl. Phys. **76**, 7778 (1994).
[7] P. Rudquist, L. Komitov, and S. T. Lagerwall, Phys. Rev. E **50**, 4735 (1994).
[8] P. Rudquist, T. Carlsson, L. Komitov, and S. T. Lagerwall, Liq. Cryst. **22**, 445 (1997).
[9] B. Musgrave, P. Lehmann, and H. J. Coles, Liq. Cryst. **26**, 1235 (1999).
[10] H. J. Coles, M. J. Clarke, S. M. Morris, B. J. Broughton, and A. E. Blatch, J. Appl. Phys. **99**, 034104 (2006).
[11] S. M. Morris, M. J. Clarke, A. E. Blatch, and H. J. Coles, Phys. Rev. E **75**, 041701 (2007).
[12] B. J. Broughton, M. J. Clarke, A. E. Blatch, and H. J. Coles, J. Appl. Phys. **98**, 034109 (2005).
[13] H. J. Coles, M. J. Coles, B. J. Broughton, and S. M. Morris, Patent No. WO/2006/003441 (2006).
[14] A. J. Davidson, S. J. Elston, and E. P. Raynes, J. Appl. Phys. **99**, 093109 (2006).
[15] R. A. Ewings, C. Kischka, L. A. Parry-Jones, and S. J. Elston, Phys. Rev. E **73**, 011713 (2006).
[16] W. den Boer, *Active Matrix Liquid Crystal Displays*, 1st ed. (Newnes, Amsterdam, 2005), Chap. 7.3, p. 186.
[17] D. W. Berreman, J. Opt. Soc. Am. **62**, 502 (1972).
[18] C. W. Oseen, Trans. Faraday Soc. **29**, 883 (1933).
[19] F. C. Frank, Discuss. Faraday Soc. **25**, 19 (1958).
[20] I. W. Stewart, *The Static and Dynamic Continuum Theory of Liquid Crystals* (Taylor & Francis, London, 2004).
[21] The notation $\mathbf{P}_{\text{flexo}}=e_s\mathbf{n}(\boldsymbol{\nabla}\cdot\mathbf{n})+e_b\mathbf{n}\times(\boldsymbol{\nabla}\times\mathbf{n})$ is also commonly used.
[22] $\epsilon_\parallel$ and $\epsilon_\perp$ are assumed to be defined at the frequency of the applied electric field (we consider a constant electric field in this paper). The parallel and perpendicular components of the refractive index, $n_\parallel$ and $n_\perp$, are defined at optical frequencies, such that in general $\epsilon_\parallel \neq n_\parallel^2$ and $\epsilon_\perp \neq n_\perp^2$. In particular the material may have $\Delta\epsilon=0$ yet be optically birefringent.
[23] G. A. DiLisi, E. M. Terentjev, A. C. Griffin, and C. Rosenblatt, J. Phys. II **3**, 597 (1993).
[24] C. Schott, S. Perkins, and H. J. Coles, Mol. Cryst. Liq. Cryst. **366**, 715 (2001).
[25] S. J. Elston, Phys. Rev. E **78**, 011701 (2008).
[26] H. G. Yoon and H. F. Gleeson, J. Phys. D **40**, 3579 (2007).
[27] For Figs. 4, 5, and 7–9 we used 500 slices per pitch of the N*. For Figs. 11 and 12 we used 100 slices per pitch.
[28] H. A. van Sprang, J. Appl. Phys. **71**, 4826 (1992).
[29] H. De Vries, Acta Crystallogr. **4**, 219 (1951).
[30] M. Abramowitz and I. A. Stegun, *Handbook of Mathematical Functions with Formulas, Graphs, and Mathematical Tables* (Dover, New York, 1964).
[31] H. J. Coles, *Handbook of Liquid Crystals*, 1st ed. (Wiley-VCH, Weinheim, 1998), Vol. 2A, p. 348.
[32] R. Lu, S. Wu, Q. Hong, and T. X. Wu, J. Disp. Technol. **1**, 3 (2005).